JMEPEG (2021) 30:1872–1884
https://doi.org/10.1007/s11665-021-05513-w

1059-9495/$19.00

Structural, Elastic Moduli, and Radiation Shielding of SiO_2-TiO_2-La_2O_3-Na_2O Glasses Containing Y_2O_3

A.F. Abd El-Rehim, H.Y. Zahran, I.S. Yahia, E.A. Abdel Wahab, and Kh.S. Shaaban

Submitted: 2 October 2020 / Revised: 8 January 2021 / Accepted: 16 January 2021 / Published online: 16 February 2021

Quaternary glasses with the chemical composition $50SiO_2$-$25TiO_2$-$5La_2O_3$- (20-x) Na_2O-xY_2O_3 by use the melt-quench method. The FT-IR spectroscopy investigated the structural change in these glasses. XRD examined the nature of these glasses. While the density is increased, the molar volume of the glass system is reduced. Ultrasonic velocities and elastic modulus of these glasses were experimentally and theoretically calculated based on the Makishima-Mackenzie model. Moreover, the radiation shielding capacity was evaluated for the studied glasses. The mass attenuation coefficient (μ/ρ), half value layer(HVL), tenth value layer (TVL), mean free path (MFP), effective atomic number (Z_{eff}), electron density (N_{eff}), equivalent atomic number Z_{eq}, and effective removal cross section (Σ_R) of prepared glasses were simulated for gamma photon energies between 0.015 and 15 MeV. Exposure build-up factor (EBF) and (EABF) of prepared glasses were evaluated.

Keywords mechanical, neutron, shielding, Yttrium

1. Introduction

Glass is a transparent, amorphous material and melts without crystallisation of an inorganic material (Ref 1–6). Sodium titanium silicate glasses have high importance in optical and electronic instruments as storage batteries. The sodium titanium silicate glasses are conventional glasses that have been developed because of their significant advantages in storage batteries (Ref 7–15). These features affected by the addition of modifiers as a transition metal and rare-earth ions. It is highly possible for applicants for UV optics and solid-state batteries because of the good ionic conductivity of these glasses (Ref 7–16). Due to the science and technology importance of sodium titanium silicate glasses, characteristics such as solid electrolytes in battery storage glasses modified with different oxides are strongly needed (Ref 17, 18). In addition, it enhances the properties of these glasses by introducing transitional oxides (Ref 19–22) or rare earth oxides (REs). Glasses containing rare-earth ions have attracted a great deal of interest because of their advantages. Lanthanum, with the symbol La and Atomic No.57. La_2O_3 has no color center in the glasses, so it is colorless. La_2O_3 enhances the chemical resistance and optical characteristics of the glass matrix. Today, the development of rare earth (RE) doped glasses for use in communication systems, such as fibers, amplifiers, and lasers, is one of the most important areas of research. Attempts were focused to improve the optics properties of RE ions in different oxides (Ref 23–28).

Depending on their concentration in the glass matrix, either as a glass modifier or a glass former, intermediate oxides such as Y_2O_3 can act. Y_2O_3 improves physical stability and other properties of doped glass matrix (Ref 29–31). The presence of TiO_2 and Y_2O_3 in glass systems influences on UV-spectroscopic because of the TiO_2 and Y_2O_3 act as an intermediate. The presence of Y_2O_3 improvement the glass-forming ability and decreases the devitrification. Because of higher density and its simple performance and lower melting temperature are several applicable titanium silicate glasses containing Y_2O_3. The photon energy of these glasses is smaller than other glasses and has a higher refractive index. Titanium borate glasses are therefore transparent, with successful optoelectronic, thermal, mechanical and chemical stability. Scientifically and technologically, the recent innovation of titanium silicate glasses containing Y_2O_3 and La_2O_3 is very significant. æTitanium silicate glasses can be regarded as an adaptable type of glass that is used in various applications because they have high thermal stability and mechanical properties. Besides, it is considered good for TMi, REi, and halides as host glasses. Due to their attractive structural, mechanical properties and infrared radiation shielding, there has been considerable interest in the study of $50SiO_2$-$25TiO_2$-$5La_2O_3$- (20-x) Na_2O-xY_2O_3 glasses over the last few years. Due to the increase in the concentration of Y_2O_3 in titanium lanthanum sodium silicate glasses, the attenuation, structural, and mechanical of these glasses can significantly increase. Furthermore, it is possible to use this glass in aircraft bodies, a shield from radiation in the x-ray canters, and facades of houses. It's the best study for the preparation of these glasses and their structural, mechanical, and shielding radiation. Thus, it is possible to find the prepared glasses are suitable for use in environments exposed to radiation. The purpose of this research is to identify the

Supplementary Information The online version contains supplementary material available at (https://doi.org/10.1007/s11665-021-05513-w).

A.F. Abd El-Rehim, H.Y. Zahran, and **I.S. Yahia**, Physics Department, Faculty of Science, King Khalid University, P.O. Box 9004, Abha 61413, Saudi Arabia; and Physics Department, Faculty of Education, Ain Shams University, P.O. Box 5101, Roxy, Cairo 11771, Egypt; **E.A. Abdel Wahab**, Physics Department, Faculty of Science, Assiut University, P.O. 71452, Assiut, Egypt; **Kh.S. Shaaban**, Chemistry Department, Faculty of Science, Al-Azhar University, P.O. 71452, Assiut, Egypt. Contact e-mail: khamies1078@yahoo.com.

attenuation proficiency of prepared glasses by Phy-X/PSD (Ref 32) software and to identify the mechanical and structure of these glasses in order to determine their suitability as gamma-ray shielding materials (Table 1).

2. Experimental Processes and Techniques

The glasses in this study were synthesized from $50SiO_2$-$25TiO_2$-$5La_2O_3$- (20-x) Na_2O-xY_2O_3 using the melt-quench technique method where x = (0,2,4,6,8,10 0, 5, 10, 15, 20, 25). The starting materials to obtain these glasses are SiO_2, Na_2CO_3, La_2O_3, Y_2O_3 and TiO_2 with high purity. All chemicals used for the glass preparation obtained from Sigma-Aldrich. The starting materials were mixed together by grinding the mixture repeatedly to obtain a fine powder. Firstly, the starting materials have been heated to 450°C for 1 h to eliminate H_2O, and CO_2. The temperature has been raised to 1200°C for 30 min. The glasses were annealed at 450 °C for 2 h to relieve the internal stresses and allowed to cool gradually to room temperature at a rate of about 30 °C h^{-1}. The weight losses were found to be less than 1%.

The amorphous state of the glasses was checked using X-ray diffraction. A Philips X-ray diffractometer PW/1710 with Ni-filtered Cu-Kα radiation (λ = 1.542 Å) powered at 40 kV and 30 mA was used.

FTIR spectra of the as-quenched glasses (after crushing them into powder form) were obtained with a Fourier transform IR spectrometer (JASCO, FT/IR–430, Japan). For this purpose, each glass powder was mixed with KBr in the proportion of 1:100 (by weight) for 20 min and pressed into a pellet using a hand press. In the wavenumber range of 4000–400 cm^{-1} with a resolution of 4 cm^{-1}, corrected for dark-current noise and normalized. The resulting spectra were curve fitted to get quantitative values for the band areas of heavily overlapped bands using a computer program Origin 8.5. Estimated error limit in the fitting process is about ± 2 cm^{-1}.

The density of each sample was measured by Archimedes' principle by using toluene as the immersion fluid. Four samples of each glass were used to determine the density (ρ). A random error in the density values was found as ± 0.025 g cm^{-1}.

The prepared samples were grinded and polished with different grades of SiC emery powder on a soft leather piece fixed on a flat platform for the ultrasonic velocity measurements. Non-parallelism of the two opposite side faces was measured with a micrometer, which could measure down to 0.01 mm. The ultrasonic velocities, longitudinal (v_L) and shear (v_T), at room temperature (∼300 K) were obtained using the pulse-echo method. In this method, x-cut and y-cut transducers (KARL DEUTSCH) operated at a fundamental frequency 4 MHz along with a digital ultrasonic flaw detector (KARL DEUTSCH Echograph model 1085) were used. The uncertainty in the measurement of the ultrasonic velocity is ±10 m s^{-1}. The two velocities besides the density were utilized to determine two independent second-order elastic constants. (See revised paper).

Table 1 Chemical composition of lithium borate glasses (mol. %)

Sample name	SiO_2	TiO_2	Na_2O	La_2O_3	Y_2O_3
	mol.%				
G1	50	25	20	5	0
G2	50	25	18	5	2
G3	50	25	16	5	4
G4	50	25	14	5	6
G5	50	25	12	5	8
G6	50	25	10	5	10

3. Results and Discussion

3.1 XRD and, FT-IR

In Fig. 1, the XRD did not demonstrate intense peak that demonstrate the high glass status of the glass samples were tested.

The FT-IR spectrum of the yttrium lanthanum titanium silicate glasses is shown in Fig. 2. Figures 3 shows the Gaussian fit of the FT-IR spectrum of these samples, respectively, are shown in Table 2. The network structural units in these glasses detected at ∼1440, ∼1180, ∼1040, ∼940, ∼850, ∼715 and ∼485 cm^{-1} (Ref 33–35). Bands in the 1442-1433 cm^{-1} region had been ascribed to antisymmetric vibrations of bridging oxygen from Si-O-Si. Bands in the 1181-1142 cm^{-1} region had been ascribed to Si-O non-bridging oxygen stretching mode. Bands in the 1058-1042 cm^{-1} region had been ascribed to Si-O-Si unit-asymmetric bridging stretching. Bands in the 873-843 cm^{-1} region had been ascribed to O-Si-O bonds' symmetric stretching vibration. Bands in the 720-712 cm^{-1} region had been ascribed to (LaO_7), (YO_8) and (TiO_6) vibrations and they overlap with the O-Si-O unit bending vibrations.

FT-IR spectral causes a shift to higher wavenumbers with an increase in yttrium concentration. In addition, it is pointed out with the increase in the concentration of yttrium, there is a high increase in the strength of the bond associated with increasing the settled glass arrangement to provide more stable structures in cooperation with yttrium in the structural network. In Table 3, the peak assignments are shown.

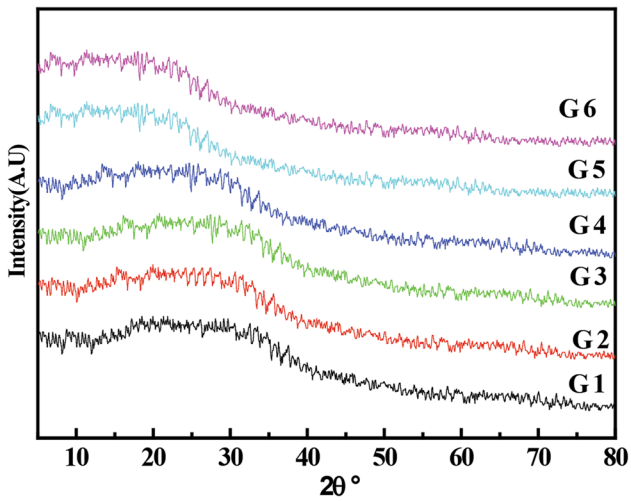

Fig. 1 XRD of the studied glasses

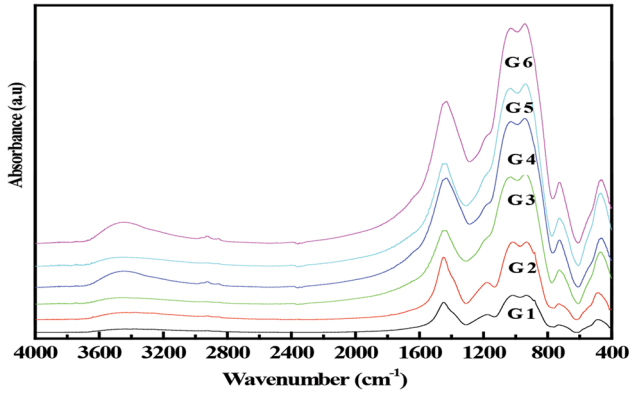

Fig. 2 Infrared spectra of the investigated glasses

3.2 Physical Features

The density of these glasses increases, and the molar volume reduces Fig. 4. The density decreased because of the difference of molecular masses between Na_2O and Y_2O_3 [61.979 & 225.81] and densities [2.27& 5.03 g/cm^3]. The reduce in molar volume because of the rise in density (Ref 21, 22).

Y^{+3} concentration was calculated as $Yi = \left(\frac{6.023\times10^{23}\, xmolfractionofcation \times valencyofcation}{Vm}\right)$. The concentration of Y^{+3} is well known to increase. Inter-ionic distance (R_i) was considered between two Y^{+3} - Y^{+3} as $R_i = \left(\frac{1}{contentofY}\right)^{\frac{1}{3}}$, It is well known that with the Y^{+3} concentration, R_i decreased because of the molar volume decrease. Y^{+3} – Y^{+3} separation ($d_{Y\text{-}Y}$) of glasses projected $(dY - Y) = \left(\frac{V_m^B}{N}\right)^{\frac{1}{3}}$ and $V_m^B = \frac{Vm}{2(1-2Xn)}$. As molar volume has decreased, ($d_{Y\text{-}Y}$) values had

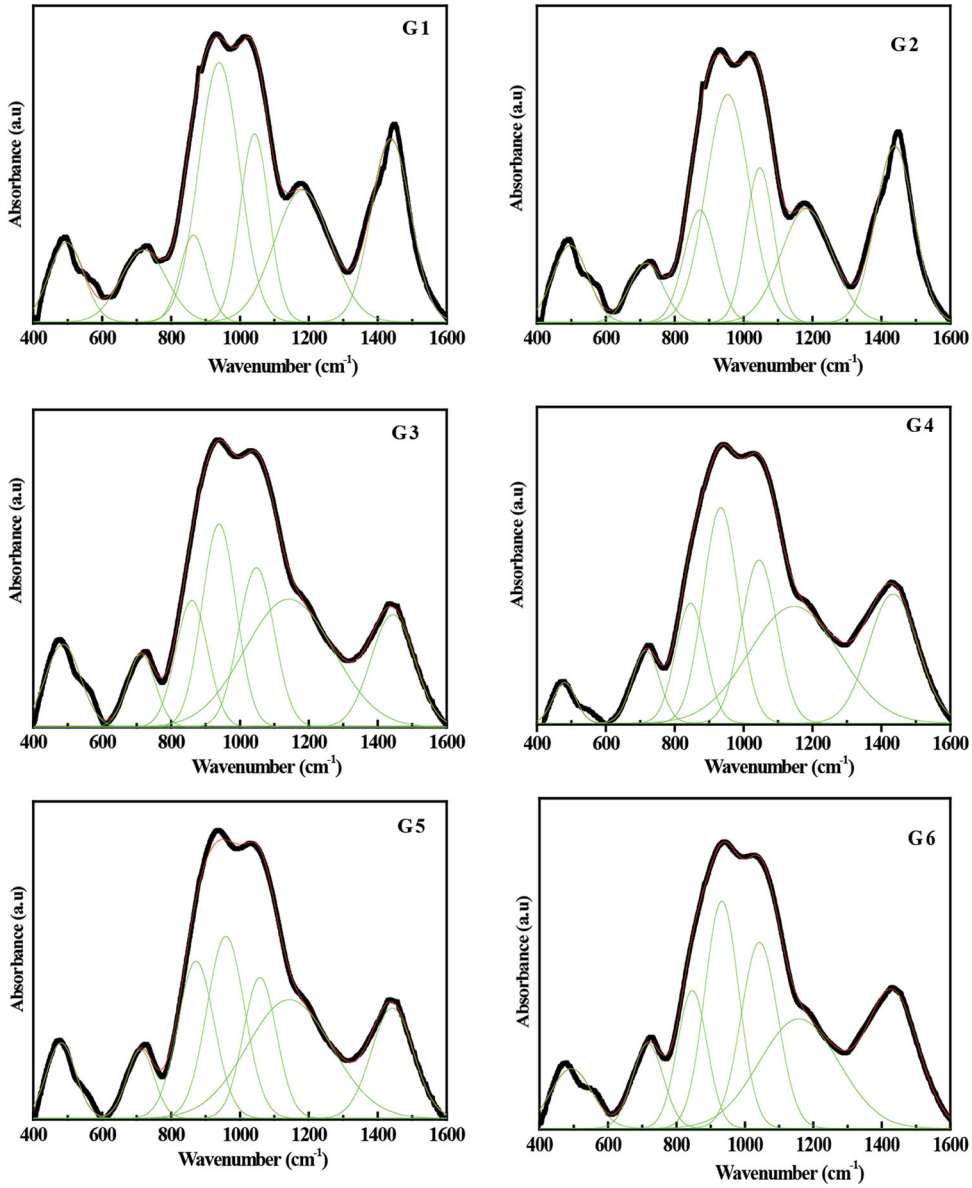

Fig. 3 Curve fitting of FT-IR spectra of the investigated glasses

Table 2 De-convolution parameter of the infrared spectra of studied glasses (C) is the component band center and (A) is the relative area (%) of the component band

G 1	C	1438	1181	1042	939	865	720	496
	A	18.5	19.03	13.97	27.16	6	8.46	6.88
G 2	C	1439	1183	1047	954	873	717	497
	A	19.2	16.7	12.3	28.3	10.24	5.76	7.5
G 3	C	1443	1142	1047	939	860	713	486
	A	12.92	29.96	15.1	18.4	10.8	5.42	7.4
G 4	C	1434	1147	1045	933	846	717	480
	A	17.15	28.72	15.8	20.6	9.8	5.4	2.53
G 5	C	1442	1143	1058	959	873	712	481
	A	12.8	27.95	13.1	19.14	16	5.1	5.91
G 6	C	1433	1158	1043	932	846	717	493
	A	17	22.28	17.6	19.92	10.58	6.7	5.92

Table 3 Peak assignments for the prepared glasses

Wave number (cm $^{-1}$)	Vibrational modes
1442-1433	Si-O-Si antisymmetric vibrations of bridging oxygen's
1181-1142	can be related to Si-O stretching mode of non-bridging oxygen's
1058-1042	Si-O-Si unit-asymmetric stretching of bridging.
873-843	is identified which is due to symmetric stretching vibration of O–Si–O bonds
720-712	are assigned to vibrations of (LaO_7), (YO_8) and (TiO_6) units and they are overlapping with bending vibrations of (O–Si–O) units.
~ 485	may be attributed to bending vibrations of Si–O–Si linkages

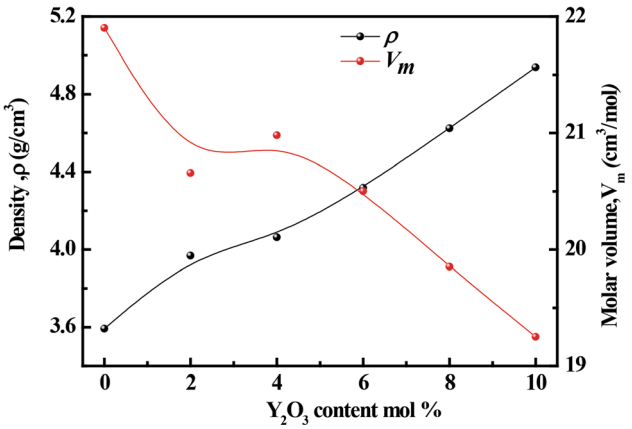

Fig. 4 Density and Molar volume of the investigated glasses

also decreased. Polaron radius r_p and inter-nuclear distance r_i were estimated as $rp = \frac{1}{2}\left(\frac{\pi}{6N}\right)^{\frac{1}{3}}$, $ri = \left(\frac{1}{N}\right)^{\frac{1}{3}}$. Because of the reduction in molar volume when Y_2O_3 has increased, these characteristics decrease. Oxygen molar volume (V_o), is estimated as, $V_o = \left(\frac{M}{\rho}\right)\left(\frac{1}{\sum xini}\right)$ and, oxygen packing density (O_{PD}) is estimated as. $OPD = \left(\frac{1000C}{Vm}\right)\left(\frac{Mol}{L}\right)$. It is noted that ($V_o$), decreased, and ($O_{PD}$) increased. These observations may be due to molar volume and glass density. Packing density estimated as $V_{i,} = \left(\frac{3\pi}{4}\right)NA\{mR_m{}^3 + nR_i{}^3\}\left(\frac{m^3}{mol}\right)$, where R_m and R_i are Pauling radii of M and O. Dissociation energy $G = (V_i{}^2 G_i)/(V_i)^{-1}$. Poisson's ratio is estimated as $\sigma = \frac{1}{2} - \left(\frac{1}{7.2*Vi}\right)$, Micro-hardness is estimated as $H = \frac{(1-2\sigma)Y}{6(1+\sigma)}$,and, Debye Temperature is assessed as $\theta_D = \frac{h}{k}\left(\frac{9N}{4\pi V_m}\right)^{\frac{1}{3}} M_s$. Average of ultrasonic velocities (M_s) is estimated as $M_s = \frac{1}{3}\left(\frac{2}{v_s^3} + \frac{1}{v_l^3}\right)^{\frac{1}{3}}$, thermal Expansion ($\alpha_P$), $\alpha_{P=23.2(\nu_L - 0.57457)}$. The mechanical constraints as (Vi), (Gi), (H), (α_P), (Z), and the connectivity to fractal bond (d) will be strongminded, these constraints are described in Table 4. This activity can be linked to the glass structure network. With the concentration of yttrium, the value of (Vi), (H), (α_P), ($_Z$), and (σ) is increased. Yet with the attentiveness of yttrium, this is correlated with the glass structure network, the importance of (Gi) is decreased. The fractal bond connectivity (d) is constant in two dimensional. Table 4 shows these values.

Using the equation, the mean number of coordinates (m) is computed $m = \sum n_{ci} X_i$ co-ordination of cations is n_{ci}. It is observed that the value of m increases with the increase in Y_2O_3. The number of bonds computed by volume of units is $n_b = \frac{N_A}{V_m}\sum n_{ci} X_i$ where $N_A$is the Avogadro number. As the content of Y_2O_3 increased, our analysis indicates that n_b was rising. There is strong evidence the role of a Y_2O_3 modifier in the glass network. Table 4 shows these values.

3.3 Mechanical Properties

Figure 5 and Table 5 represented sound velocities of prepared glasses. This found that Y_2O_3 increase those veloc-

Table 4 Various physical parameters of the studied glasses

Samples	G 1	G 2	G 3	G 4	G 5	G 6
Packing density (*Vi*), (cm^3/mol)	0.65	0.695	0.7	0.712	0.74	0.77
Dissociation energy (*Gi*),	10.52	10.85	11.19	11.53	11.87	12.2
Oxygen molar volume (*Vo*), (cm^3/mol)	11.84	10.7	10.44	9.81	9.15	8.56
Oxygen packing density (O_{PD}), mol/L	84.5	93.43	95.8	101.9	109.3	116.88
Fractal bond connectivity (d)	1.8	1.8	1.827	1.83	1.848	1.83
Thermal expansion coefficient (α_P), K^{-1}	124571	125267	125615	126195	126891	127819
POISSON'S ratio(σ), a. u	0.286	0.3	0. 3	0.305	0.31	0.32
Debye temperatures (K)	448.5	466	472.85	485	499.58	513. 4
Microhardness (H), G_{Pa}	3.81	4.25	4.47	4.81	5.24	5.62
Softening temperature (K)	802.2	823.13	846.7	867.16	890.4	910.4
Acoustic impedance (Z)/ (10^7 kg m^{-2} s^{-1})	1.02	1.14	1.17	1.25	1.35	1.45

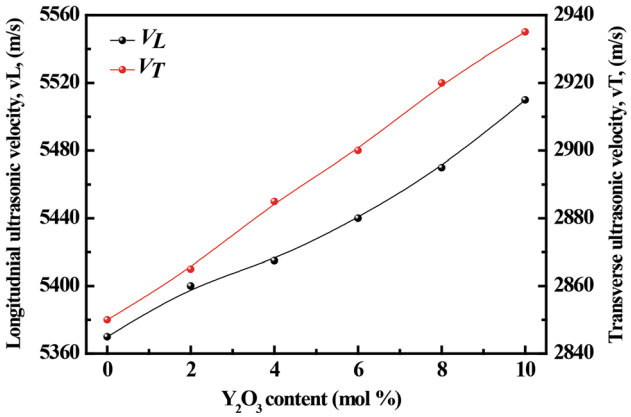

Fig. 5 Dependence of the longitudinal and shear ultrasonic velocities v_L and v_T of the investigated glasses against of Y_2O_3 by mol. %

ities, because of increased density and cross-link density (Ref 33–36). v_L ranges between 5370 and 5510 m/s and v_T ranges between 2850 and 2935m/s. According to the previous FTIR analysis, with an increasing in Y_2O_3 contented, band position shifted to a higher wavenumber, this shift caused the composition change in the glass network and increased the glass network connectivity.

To estimate elastic-modules as, $L = \rho v_l^2$, $G = \rho v_s^2$, $Y = (1+\sigma)2G, and,$ $K = L - \left(\frac{4}{3}\right)G$. Elastic-modulus of glasses have been estimated and represented in Fig. 6 (A,B) and Table 5. It indicated that, are increasing with the increasing of Y_2O_3 content. It is because of the transformation of Si-O-Na into Si-O-Y , and Na-O bond strength (20KCal/mol) is much lower than Y-O (50KCal/mol) (Ref 37). This behavior is linked to the modification of the coordination number with Y_2O_3 increase, the growth in average constant force and cross-link density. As Y_2O_3 increases at the expense of Na_2O, the molar volume decreases, and the density increases, making the glass structure more compact.

3.4 Mass Attenuation Coefficient (I/q).

The (μ/ρ) has been estimated as $\left(\frac{\mu}{\rho}\right) = \sum_i w_i \left(\frac{\mu}{\rho}\right)_i$. Figure 7 represented the (μ/ρ) as a function of photon energy, and yttrium concentrations . It is shown that the (μ/ρ) of prepared samples increased at small energy, then it has remained constant at higher energy (Ref 38–44). It designated that the Y_2O_3 increases when (μ/ρ) increases. This increase is associated to density. Thus, the adding of Y_2O_3 enhances γ- radiation attenuation. Table 6 represents the comparison the (μ/ρ) of sample number G6 with the other glasses.

3.5 (HVL), (TVL) and (MFP)

The mean free path (MFP) has been projected $MEP = \left(\frac{1}{\mu}\right)$. The tenth (TVL) and half-value layer (HVL) determined by $TVL = \left(\frac{ln10}{\mu}\right)$, $HVL = \left(\frac{ln2}{\mu}\right)$. Fig. 8, 9 and 10 shows values of these parameters of prepared samples. These values are increased at the photon energy increased rendering to achieve results. As Y_2O_3 rise, these parameters values are reducing as well. Hence the addition of Y_2O_3 enhances γ- radiation attenuation. The comparison of (HVL) and (MFP) with standard materials was represented in Fig. 11(A, B). These glasses have been found to have a high radiation absorption factor of γ- over the other glasses (Ref 38–44).

3.6 (Z_{eff}) (N_{eff}) and Z_{eq} of prepared glasses.

The effective atomic number (Z_{eff}) estimated as $Z_{eff} = \left(\frac{\sigma_a}{\sigma_e}\right)$ where (σ_a) the atomic cross sections $\sigma_a \sigma_a = \sigma_m \frac{1}{\sum_i n_i} = \left(\frac{\mu}{\rho}\right)_{target} / N_A \sum_i \frac{w_i}{A_i}$, and σ_e the electronic cross sections $\sigma_e = \frac{1}{N}\sum_i \left(\frac{\mu}{\rho}\right)_i \frac{f_i w A_i}{z_i}$. Fig. 12 shows the Z_{eff} of the studied glasses, which diverse with γ-energy and with the yttrium concentrations. Because of the communication of the photoelectric at this range, Z_{eff} is suggested to have a greater value for these glasses with low energy. Because of X-ray K-edges, the Z_{eff} values gradually increase at higher energy. Glass G 6, because of the replacement of Na_2O by Y_2O_3, has a higher Z_{eff} value. The inclusion of Y_2O_3 to glasses increases the attenuation rate for these glasses (Ref 38–44).

Electron density (N_{eff}) was projected $N_{eff} = N\frac{Z_{eff}}{\sum_i F_i A_i}$. Figure 13 represented the (N_{eff}) values of formulated glasses against energy and Y_2O_3 concentrations. At lower energy, it is noticed that (N_{eff}) reduced and then increased slowly. The Compton scattering interaction is responsible for this decrease. Thus, the addition of Y_2O_3 enhances γ- radiation attenuation. This statement is associated to pair creation effect in higher energy and an increase in the content of Y_2O_3.

Table 5 Values of sound velocities (v_L and v_T), elastic moduli calculated, and theoretically of the studied glasses

Sample no.	v_L (m s^{-1})	v_T	L	G	K	Y	L_{Th} (Gpa)	G_{Th}	K_{Th}	Y_{Th}
G 1	5370	2850	103.6	29.18	64.7	76.11	76	23.7	44.4	57.16
G 2	5400	2865	115.7	32.57	72.2	84.95	86.87	25.9	52.4	63
G 3	5415	2885	119	33.82	74	88.05	88.56	26.5	53.3	64.55
G 4	5440	2900	127.7	36.31	79.3	94.53	95.7	28	58.4	68.61
G 5	5470	2920	138.3	39.43	85.7	102.57	104.9	29.8	65.1	73.51
G 6	5510	2935	149.9	42.55	93.2	110.78	114. 7	31.7	72.4	78.6

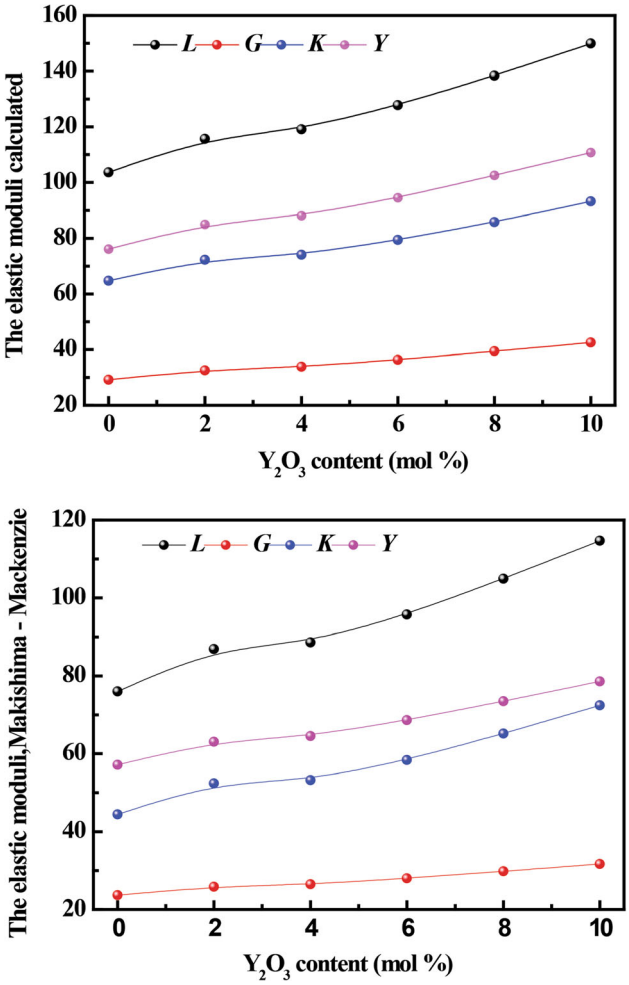

Fig. 6 (a) Composition dependence of the elastic modulus measured of the studied glasses against of Y_2O_3 by mol.%. (b) Composition dependence of the elastic modulus theoretically of the studied glasses against of Y_2O_3 by mol.%

Equivalent atomic number Z_{eq} was projected as $Zeq = \frac{Z1(logR2-logR)+Z2(logR-logR1)}{logR2-logR1}$. Fig. 14 symbolised the (Z_{eq}) of glasses in range 0.015 and 15 MeV. It showed that (Zeq) enhanced with the photon energy incident and with the replacement of Y_2O_3 with Na_2O. (Z_{eq}) decreased with energy and Y_2O_3 content because of the interaction of Compton

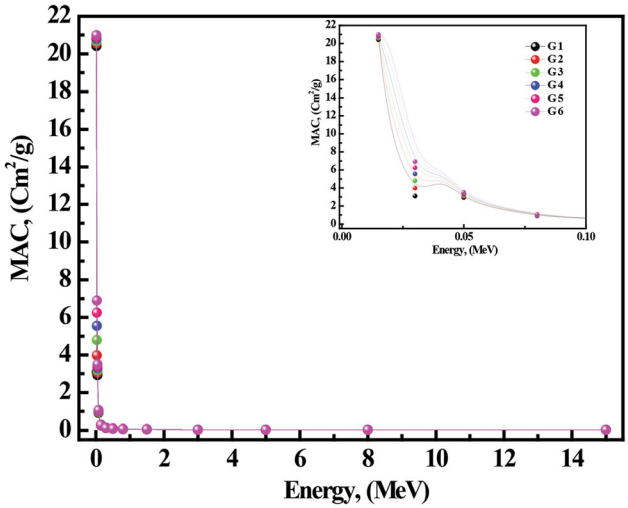

Fig. 7 The mass attenuation coefficient (μ/ρ) of prepared glasses as a function of photon energy

scattering. The highest (Zeq) value at 1 MeV. The (Zeq) value is reduced at higher energy than 1 MeV because of pair creation interaction (Ref 38–44).

3.7 Exposure Build-up Factor (EBF) and (EABF) of Prepared Glasses

G–P fitting parameters have been estimated as $P = \frac{P1(logZ2-logZeq)+Z2(logZeq-logZ1)}{logZ2-logZ1}$ where P_1 and P_2 are the G–P-fitting parameters. EABF and EBF have been projected by using G–P fitting $B(E,X) = 1 + \frac{b-1}{K-1}(K^x - 1)$ for K $\neq 1$, $B(E,X) = 1 + (b-1)x$ K $= 1$ where $K(E,X) = cx^a + d\frac{tanh(\frac{x}{Xk}-2)-tanh(-2)}{1-tanh(-2)}$. EBF and, EABF are obtained from GP-fitting. Figs. (15 and 16) symbolized the (EBF) and EABF of glasses against the gamma energy. The values of EBF and EABF are affected by the energy and composition of the glass samples (Ref 38–44). EBF and EABF values are small at the lower energy because the energy photons will be absorbed by the glasses and then expanded with the energy increase because of Compton scattering. After that, EBF and EABF decrease with increasing energy because of pair production. In addition, enhanced protective properties such as G 6 glass should be achieved with the Y_2O_3 content of studied glasses (Tables 7 and 8).

Table 6 Mass attenuation coefficients (in cm^2/g) in comparison with different glass samples

Samples	MAC, (MeV) 0.02	10
G6 [Present work]	20.429	0.028
$66B_2O_3$-$5Al_2O_3$-$29Na_2O$	1.074	0.020
$5Bi_2O_3$-$61B_2O_3$-$5Al_2O_3$-$29Na_2O$	5.059	0.022
$10Bi_2O_3$-$56B_2O_3$- $5Al_2O_3$-$29Na_2O$	9.043	0.023
$0PbO$-$30SiO_2$-$46.67B_2O_3$-$23.33Na_2O$	1.386	0.023
$5PbO$-$25SiO_2$-$46.67B_2O_3$-$23.33Na_2O$	5.167	0.021
$10PbO$-$20SiO_2$-$46.67B_2O_3$-$23.33Na_2O$	8.952	0.024
$49.46SiO_2$- $26.38Na_2O$- $23.08CaO$- $1.07P_2O_5$	3.982	0.024
$47.84SiO_2$- $26.67Na_2O$- $23.33CaO$- $2.16P_2O_5$	3.985	0.023
$44.47SiO_2$- $27.26Na_2O$- $23.85CaO$- $4.42P_2O_5$	4.057	0.024
$40.96SiO_2$- $27.87Na_2O$- $24.39CaO$- $6.78P_2O_5$	4.113	0.024
$37.28SiO_2$- $28.52Na_2O$- $24.95CaO$- $9.25P_2O_5$	4.061	0.024
$48.98SiO_2$- $26.67Na_2O$- $23.33CaO$- $1.02P_2O_5$	3.983	0.023
$43.66SiO_2$- $28.12Na_2O$- $24.60CaO$- $3.62P_2O_5$	4.100	0.024
$38.14SiO_2$- $29.62Na_2O$- $25.91CaO$- $6.33P_2O_5$	4.190	0.022
$40.71SiO_2$- $28.91Na_2O$- $25.31CaO$-5.07 P_2O_5	4.131	0.022

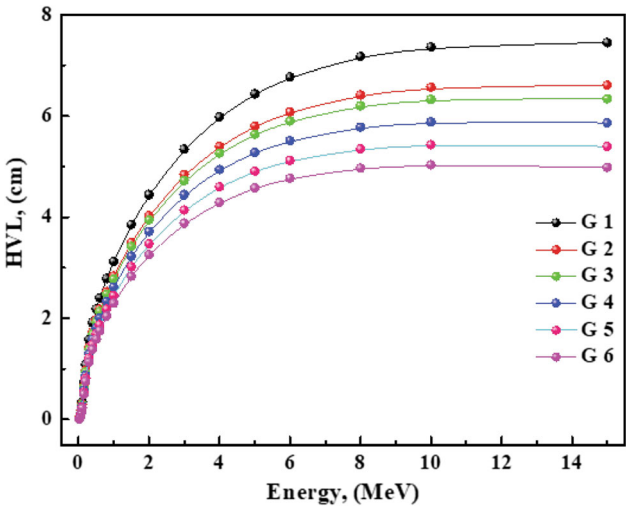

Fig. 8 The half value layer of prepared glasses as a function of photon energy

3.8 Fast Neutron Removal Cross Section (FNRCS) (1/cm)

Effective removal cross section (Σ_R),projected: $\left(\frac{\Sigma_R}{\rho}\right) = \sum_i w_i \left(\frac{\Sigma_R}{\rho}\right)_i$ and $R = \sum_i \rho_i \left(\frac{R}{\rho}\right)_i$. Fig. 17 ($\Sigma_R$) of glass samples against gamma energy was illustrated. At small energy, it is noticed that the (Σ_R) increased. Small variations of these glasses with a decrease in the value of (Σ_R) are obtained at higher energy because of increased Y_2O_3 at the expense of Na_2O. In our sample (Y_2O_3: 225.81) increased in prepared glasses. The increase in the Y_2O_3 content may lead to an improvement in the shielding of neutrons. The increase in Y_2O_3 enhances ΣR values; therefore, we can say that the addition of Y_2O_3 to glasses improves the γ -radiation attenuation (Ref 38–44).

Figure 18 shows the FNRCS of the prepared glasses. It is observed that the FNRCS values are increased as the Y_2O_3 content increased. The rise in FNRCS is influenced by the composition and density of glass. So, we can say that the addition of Y_2O_3 to prepare glasses increase the FNRCS. $Ti =$

$$\left(\frac{6.023\times10^{23}\, x\, molfractionofcation\times valencyofcation}{Vm}\right) \qquad Ti =$$
$$\left(\frac{6.023\times10^{23}\, x\, molfractionofcation\times valencyofcation}{Vm}\right)$$

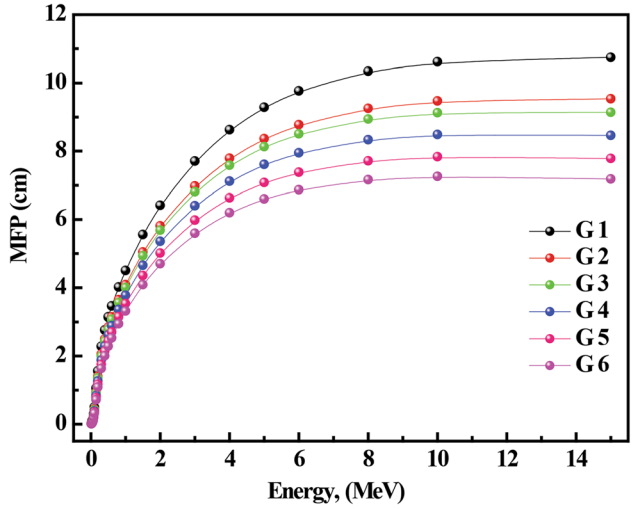

Fig. 9 The MFP of prepared glasses as a function of photon energy

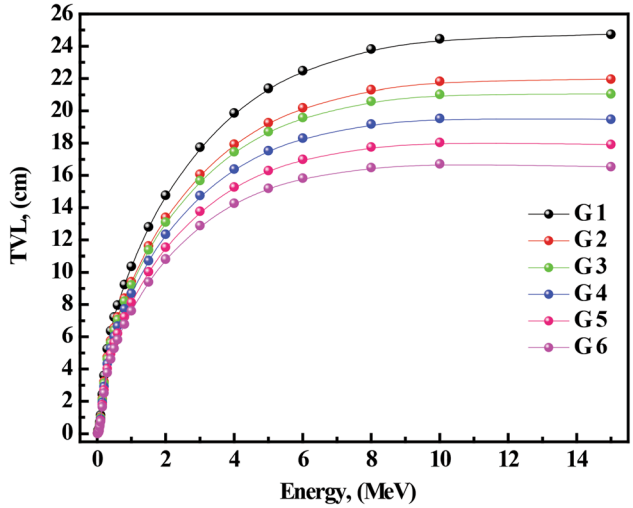

Fig. 10 The tenth value layer (TVL) of prepared glasses as a function of photon energy

4. Conclusions

In the present investigation, six glasses of titanium lanthanum sodium silicate glasses containing different amount of yttrium with the chemical composition $50SiO_2$-$25TiO_2$-$5La_2O_3$- (20-x) Na_2O-xY_2O_3 where $x = (0 \leq x \geq 10$ $0, 5, 10, 15, 20, 25)$ have been fabricated by conventional melt-quenching method. The structure, mechanical, and shield-

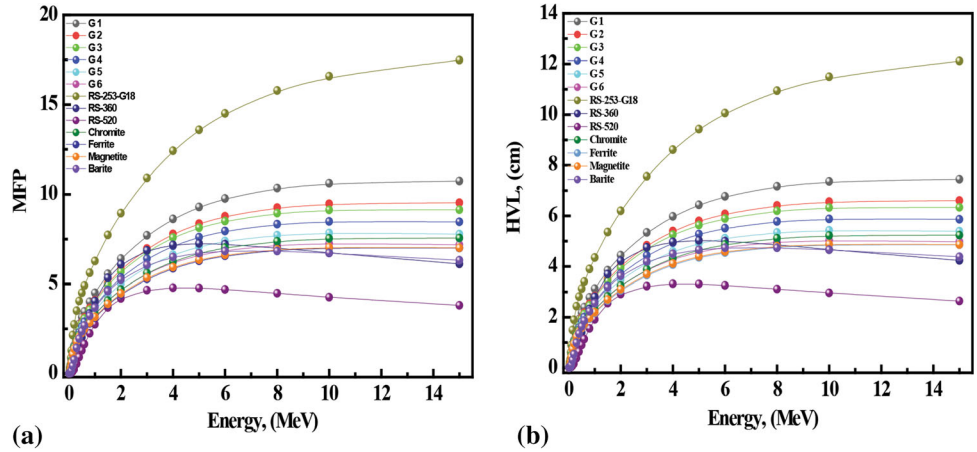

Fig. 11 (a) The comparison of MFP (cm) for the prepared glasses as a function of photon energy with standard materials. (b) The comparison of half value layer (cm) for the prepared glasses as a function of photon energy with standard materials

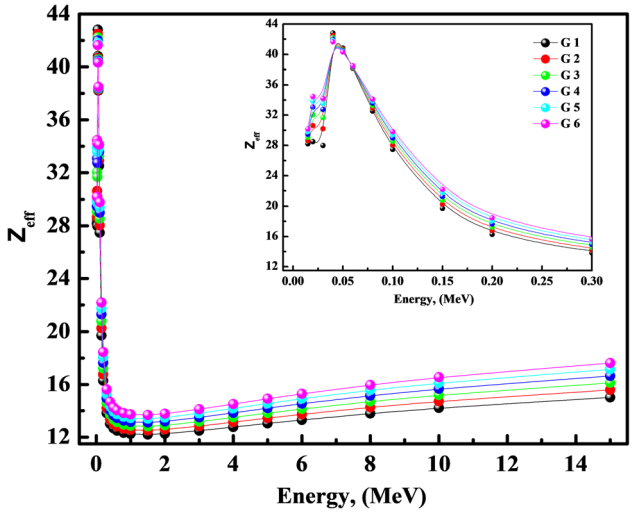

Fig. 12 The effective atomic number (Z_{eff}) of prepared glasses as a function of photon energy

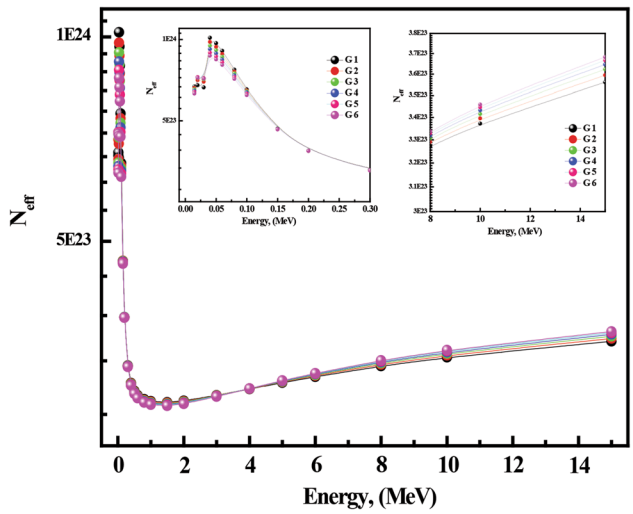

Fig. 13 The electron density (N_{eff}) of the prepared glasses as a function of photon energy

ing parameters for these glasses were investigated. The results reveal the following items:

1. The amorphous nature of glasses was confirmed by XRD measurements.
2. The structural changes of the studied glass have been estimated via FTIR spectroscopy.
3. FT-IR spectral pointed out with the increase in the concentration of yttrium, there is a high increase in the strength of the bond associated with increasing the settled glass arrangement to provide more stable structures in cooperation with yttrium in the structural network.
4. The density of the samples was increased with increasing Y_2O_3 concentration while the molar volume decreased.
5. The ultrasonic velocities these glasses were increased with increasing Y_2O_3 concentration
6. Elastic modulus of these glasses was experimentally and theoretically calculated based on the Makishima-Mackenzie model is increased.

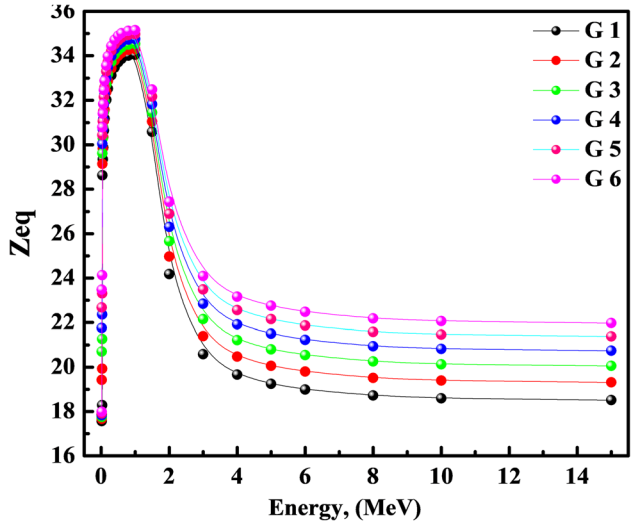

Fig. 14 Equivalent atomic number (Z_{eq}) of the prepared glasses as a function of photon energy

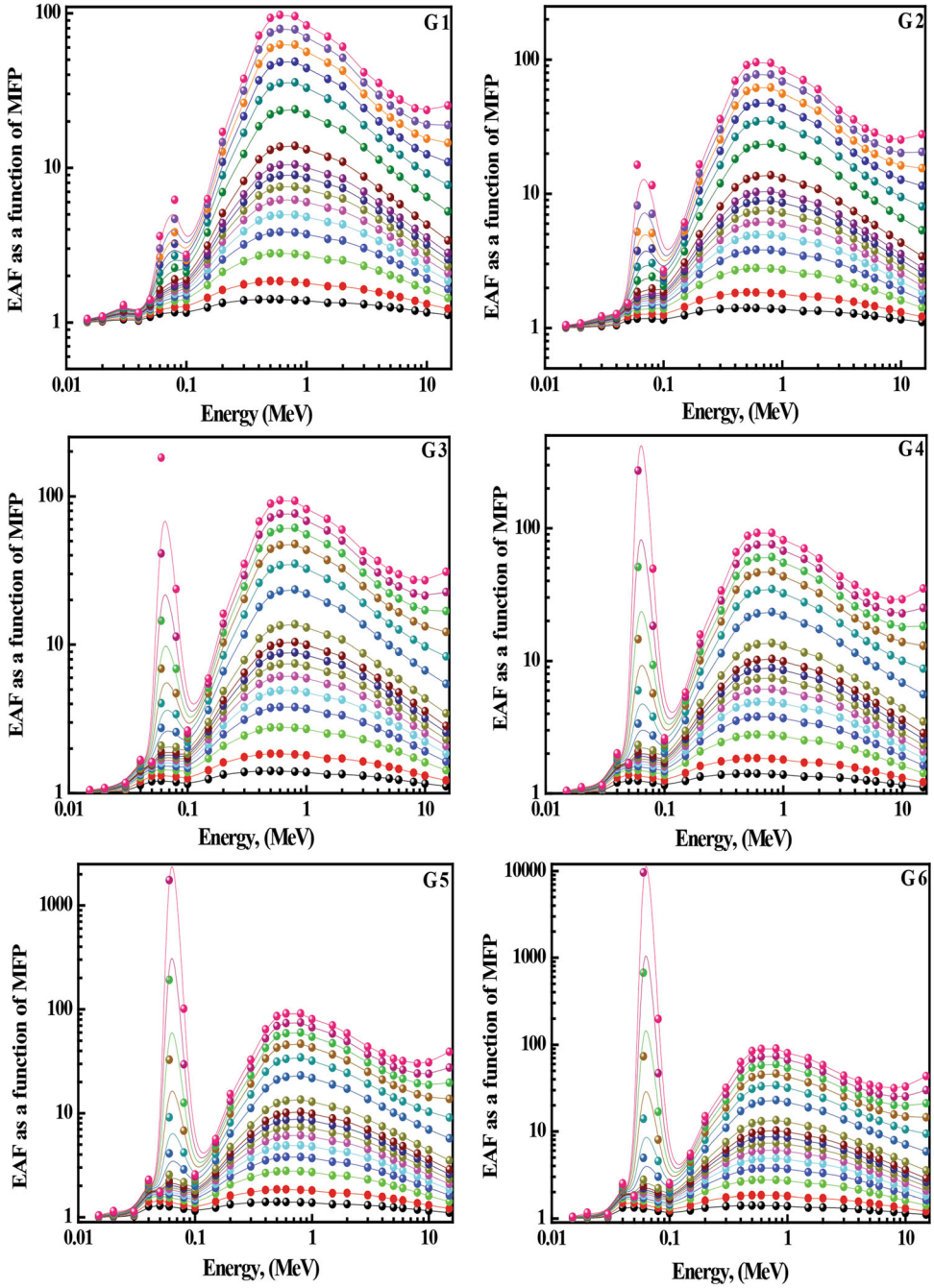

Fig. 15 Variation of EBF versus the gamma ray energy for the prepared glasses as a function of photon energy

7. The gamma shielding features of the proposed glasses were estimated using Phy-X / PSD program between 0.015 and 15 MeV. The effect of the addition of Y_2O_3 on the shielding ability of the glasses was discussed and we found that: (i) The mass attenuation coefficient increased with the increase in the concentration of Y_2O_3 from 0 mol. % to 10 mol. %, (ii) The addition of Y_2O_3 can improve the shielding effectiveness the glasses, and (iii) The sample coded as G 6 possesses the lowest HVL while highest Z_{eff}.

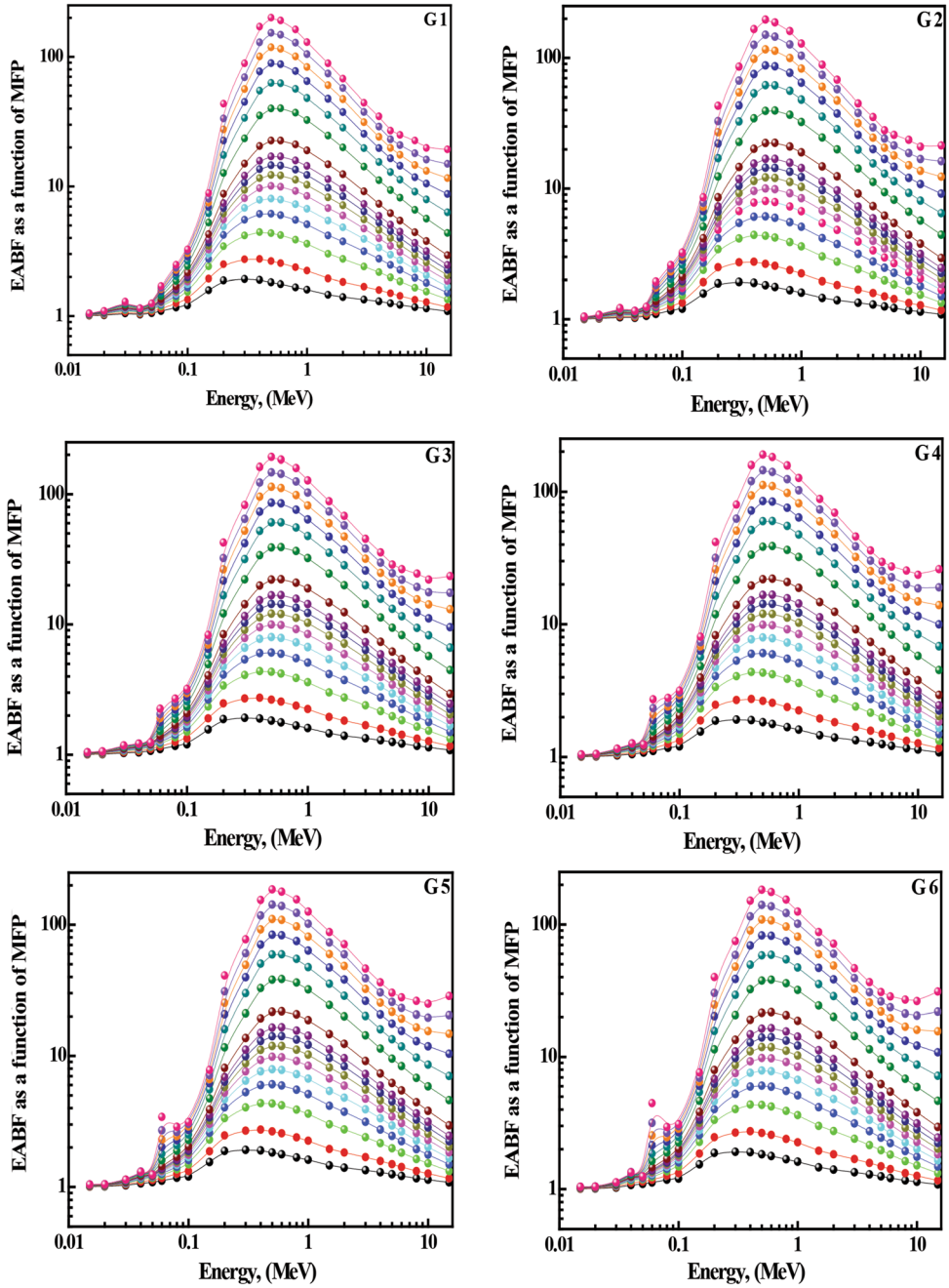

Fig. 16 Variation of EABF versus the gamma ray energy for the prepared glasses as a function of photon energy

Table 7 G-P Fitting Parameters for EBF, and G-P Fitting Parameters for EABF of glass name G 1.

	G-P Fitting Parameters for EBF					G -P Fitting Parameters for EABF				
Energy (MeV)	**a**	**b**	**c**	**d**	**Xk**	**a**	**b**	**c**	**d**	**Xk**
1.50E-02	0.142	1.009	0.494	− 0.284	29.256	0.174	1.010	0.453	− 0.260	25.644
2.00E-02	0.291	1.013	0.302	− 0.249	15.511	0.158	1.023	0.455	− 0.314	30.471
3.00E-02	0.248	1.035	0.331	− 0.178	17.147	0.250	1.077	0.346	− 0.147	13.199
4.00E-02	0.182	1.111	0.380	− 0.249	25.089	0.203	1.040	0.385	− 0.269	24.045
5.00E-02	0.158	1.138	0.288	− 0.084	11.905	0.230	1.081	0.343	− 0.132	12.744
6.00E-02	0.388	1.173	0.260	− 0.160	14.626	0.294	1.137	0.315	− 0.153	14.560
8.00E-02	0.325	1.262	0.300	− 0.155	14.284	0.270	1.254	0.348	− 0.138	14.338
1.00E-01	0.199	1.318	0.442	− 0.115	17.510	0.171	1.344	0.483	− 0.103	18.321
1.50E-01	0.239	1.855	0.412	− 0.146	13.743	0.229	1.940	0.432	− 0.143	13.668
2.00E-01	0.205	2.465	0.516	− 0.138	13.698	0.181	2.503	0.558	-0.126	13.630
3.00E-01	0.095	2.676	0.753	− 0.072	13.384	0.082	2.732	0.791	− 0.067	13.253
4.00E-01	0.053	2.738	0.897	− 0.059	13.025	0.042	2.750	0.932	− 0.054	12.857
5.00E-01	0.023	2.654	0.994	− 0.042	12.728	0.015	2.646	1.025	− 0.037	12.509
6.00E-01	0.010	2.567	1.039	− 0.034	12.275	0.003	2.551	1.066	− 0.031	12.001
8.00E-01	− 0.003	2.391	1.084	− 0.027	11.306	− 0.008	2.370	1.105	− 0.025	10.881
1.00E+00	− 0.010	2.254	1.102	− 0.021	10.464	− 0.014	2.233	1.120	− 0.019	9.906
1.50E+00	− 0.021	1.949	1.132	− 0.010	9.801	− 0.023	1.950	1.141	− 0.009	8.937
2.00E+00	− 0.023	1.831	1.124	0.001	17.591	− 0.027	1.829	1.137	0.007	23.127
3.00E+00	0.000	1.685	1.039	− 0.016	12.304	− 0.004	1.687	1.048	− 0.011	12.004
4.00E+00	0.015	1.576	0.988	− 0.028	13.166	0.016	1.589	0.980	− 0.024	12.068
5.00E+00	0.022	1.487	0.966	− 0.035	14.363	0.023	1.500	0.958	− 0.035	13.385
6.00E+00	0.026	1.413	0.959	− 0.037	13.586	0.028	1.432	0.945	− 0.035	12.783
8.00E+00	0.034	1.318	0.942	− 0.040	13.020	0.034	1.336	0.931	− 0.033	12.157
1.00E+01	0.043	1.259	0.924	− 0.050	14.045	0.046	1.282	0.898	− 0.049	13.898
1.50E+01	0.039	1.160	0.956	− 0.043	14.528	0.037	1.175	0.941	− 0.040	14.457

Table 8 G-P Fitting Parameters for EBF, and G-P Fitting Parameters for EABF of glass name G 6.

	G-P Fitting Parameters for EBF					G -P Fitting Parameters for EABF				
Energy (MeV)	**a**	**b**	**c**	**d**	**Xk**	**a**	**b**	**c**	**d**	**Xk**
1.50E-02	0.142	1.009	0.494	− 0.285	29.250	0.142	1.009	0.494	− 0.284	29.256
2.00E-02	0.449	1.014	0.251	− 0.409	11.195	0.291	1.013	0.302	− 0.249	15.511
3.00E-02	0.200	1.036	0.373	− 0.260	24.259	0.248	1.035	0.331	− 0.178	17.147
4.00E-02	0.215	1.511	0.329	− 0.086	15.894	0.182	1.111	0.380	− 0.249	25.089
5.00E-02	0.123	1.508	0.285	− 0.099	12.691	0.158	1.138	0.288	− 0.084	11.905
6.00E-02	0.455	1.436	0.273	− 0.138	14.543	0.388	1.173	0.260	− 0.160	14.626
8.00E-02	0.367	1.332	0.320	− 0.154	14.101	0.325	1.262	0.300	− 0.155	14.284
1.00E-01	0.207	1.243	0.437	− 0.114	13.843	0.199	1.318	0.442	− 0.115	17.510
1.50E-01	0.129	1.409	0.602	− 0.069	14.160	0.239	1.855	0.412	− 0.146	13.743
2.00E-01	0.104	1.601	0.698	− 0.063	13.906	0.205	2.465	0.516	− 0.138	13.698
3.00E-01	0.040	1.737	0.888	− 0.030	13.428	0.095	2.676	0.753	− 0.072	13.384
4.00E-01	0.009	1.812	1.016	− 0.023	12.781	0.053	2.738	0.897	− 0.059	13.025
5.00E-01	− 0.007	1.841	1.084	− 0.017	12.122	0.023	2.654	0.994	− 0.042	12.728
6.00E-01	− 0.015	1.842	1.118	− 0.014	11.280	0.010	2.567	1.039	− 0.034	12.275
8.00E-01	− 0.022	1.825	1.147	− 0.012	10.642	− 0.003	2.391	1.084	− 0.027	11.306
1.00E+00	− 0.023	1.799	1.146	− 0.011	10.565	− 0.010	2.254	1.102	− 0.021	10.464
1.50E+00	− 0.035	1.700	1.178	0.008	14.918	− 0.021	1.949	1.132	− 0.010	9.801
2.00E+00	− 0.021	1.704	1.122	− 0.005	8.426	− 0.023	1.831	1.124	0.001	17.591
3.00E+00	− 0.007	1.631	1.062	− 0.011	12.354	0.000	1.685	1.039	− 0.016	12.304
4.00E+00	0.006	1.562	1.019	− 0.018	12.542	0.015	1.576	0.988	− 0.028	13.166
5.00E+00	0.014	1.496	0.996	− 0.024	13.166	0.022	1.487	0.966	− 0.035	14.363
6.00E+00	0.023	1.451	0.970	− 0.033	13.270	0.026	1.413	0.959	− 0.037	13.586
8.00E+00	0.030	1.367	0.955	− 0.039	13.571	0.034	1.318	0.942	− 0.040	13.020
1.00E+01	0.039	1.307	0.940	− 0.048	13.739	0.043	1.259	0.924	− 0.050	14.045
1.50E+01	0.050	1.212	0.931	− 0.057	14.075	0.039	1.160	0.956	− 0.043	14.528

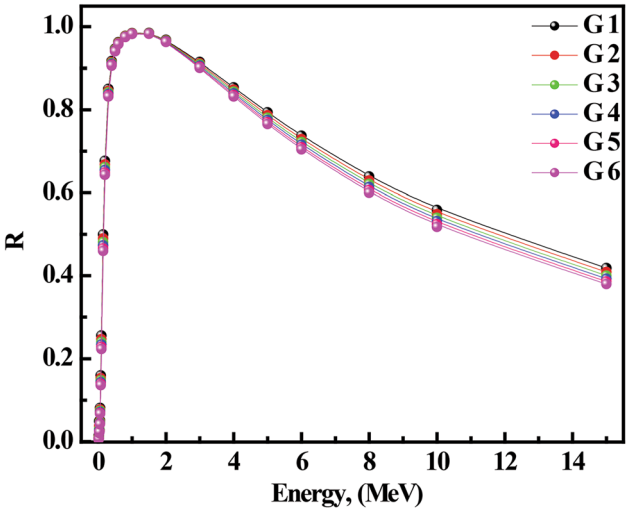

Fig. 17 Effective removal cross-through (ΣR) for the prepared glasses as a function of photon energy

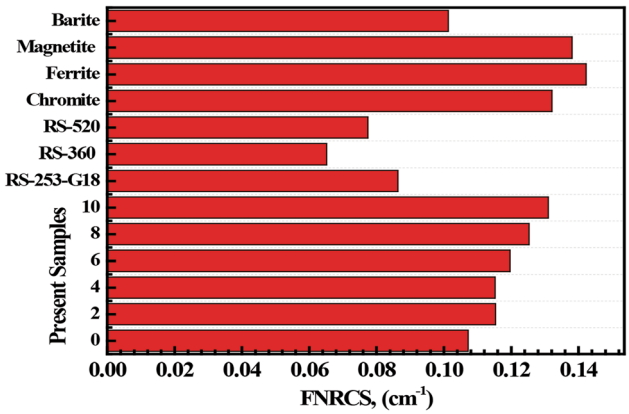

Fig. 18 FNRCS for the prepared glasses comparison with standard materials

Achieved results revealed that the increase in the concentration of Y_2O_3 in SiO_2-La_2O_3-TiO_2-Na_2O-Y_2O_3 glass system can lead to a significant improvement in the structural, mechanical, and gamma photons attenuation. In addition, theses glass can be used as in aircraft bodies, a shield from radiation in the x-ray centers, facades of houses photoelectric, optoelectronic, nonlinear optical devices and optical instruments like solar cells and wave guide-based optical circuits.

Acknowledgments

The authors extend their appreciation to the Deanship of Scientific Research at King Khalid University for funding this work through research groups program under grant number R.G.P. 2/93/41

Conflict of interest

The Authors declare that they have no conflict of interest.

Ethical Approval

This article does not contain any studies with human participants or animals performed by any of the authors.

Informed Consent

Informed Consent was obtained from all individual participants included in the study.

References

1. D.R. Messier, Preparation and Properties of Y-Si-Al-O-N Glasses, *Int. J. High Technol. Ceram.*, 1987, **3**(1), p 33–41. https://doi.org/10.1016/0267-3762(87)90061-0
2. K.S. Shaaban, E.A.A. Wahab, E.R. Shaaban et al., Electronic Polarizability, Optical Basicity, Thermal, Mechanical and Optical Investigations of ($65B_2O_3$–$30Li_2O$–$5Al_2O_3$) Glasses Doped with Titanate, *J. Elec. Mater.*, 2020, **49**, p 2040–2049. https://doi.org/10.1007/s11664-019-07889-x
3. K.S. Shaaban, S.M. Abo-Naf and M.E.M. Hassouna, Physical and Structural Properties of Lithium Borate Glasses Containing MoO_3, *Silicon*, 2019, **11**, p 2421–2428. https://doi.org/10.1007/s12633-016-9519-4
4. E.A. Abdel Wahab, K.S. Shaaban, R. Elsaman et al., Radiation Shielding, and Physical Properties of Lead Borate Glass Doped ZrO_2 Nanoparticles, *Appl. Phys. A*, 2019, **125**, p 869. https://doi.org/10.1007/s00339-019-3166-8
5. W.M. Abd-Allah, H.A. Saudi, K.S. Shaaban et al., Investigation of Structural and Radiation Shielding Properties of $40B_2O_3$–30PbO–(30–*x*) BaO-*x* ZnO Glass System, *Appl. Phys. A*, 2019, **125**, p 275. https://doi.org/10.1007/s00339-019-2574-0
6. K.S. Shaaban, S.M. Abo-naf, A.M. Abd Elnaeim and M.E.M. Hassouna, *Studying Effect of MoO_3 on Elastic and Crystallization Behavior of Lithium Diborate Glasses on Elastic and Crystallization Behavior of Lithium Diborate Glasses*, Phys. A, Appl, 2017. https://doi.org/10.1007/s00339-017-1052-9
7. I. Hussain, E.K. Barimah, Y. Iqbal, G. Jose and R. Muhammad, Thermal, Mechanical and Optical Properties of TiO_2-doped Sodium Silicate Glass-Ceramics, *Trans. Indian Ceram. Soc.*, 2019 https://doi.org/10.1080/0371750x.2019.1626287
8. E.A.A. Wahab and K.S. Shaaban, Effects of SnO_2 on Spectroscopic Properties of Borosilicate Glasses Before and After Plasma Treatment and its Mechanical Properties, *Mater. Res. Express*, 2018, **5**(2), p 025207. https://doi.org/10.1088/2053-1591/aaaee8
9. M. Rezvani, B. Eftekhari-Yekta, M. Solati-Hashjin and V.K. Marghussian, Effect of Cr_2O_3, Fe_2O_3 and TiO_2 Nucleants on the Crystallization Behaviour of SiO_2–Al_2O_3–CaO–MgO(R_2O) Glass-Ceramics, *Ceram. Int.*, 2005, **31**(1), p 75–80. https://doi.org/10.1016/j.ceramint.2004.03.037
10. S. Banijamali, B. Eftekhari Yekta, H.R. Rezaie and V.K. Marghussian, Crystallization and Sintering Characteristics of CaO–Al_2O_3–SiO_2 Glasses in the Presence of TiO_2, CaF_2 and ZrO_2, *Thermochim. Acta*, 2009, **488**(1–2), p 60–65. https://doi.org/10.1016/j.tca.2008.12.031
11. K. Shaaban, E.A. Abdel Wahab, A.A. El-Maaref et al., Judd-Ofelt Analysis and Physical Properties of Erbium Modified Cadmium Lithium Gadolinium Silicate Glasses, *J. Mater. Sci. Mater. Electron*, 2020, **31**, p 4986–4996. https://doi.org/10.1007/s10854-020-03065-8
12. K.S. Shaaban, E.S. Yousef, E.A. Abdel Wahab et al., Investigation of Crystallization and Mechanical Characteristics of Glass and Glass-Ceramic with the Compositions *x*Fe_2O_3-$35SiO_2$-$35B_2O_3$-$10Al_2O_3$-(20–*x*) Na_2O, *J. Mater. Eng. Perform.*, 2020 https://doi.org/10.1007/s11665-020-04969-6
13. A.A. El-Maaref, S. Badr, K.S. Shaaban, E.A.A. Wahab and M.M. ElOkr, Optical Properties and Radiative Rates of Nd^{3+} Doped Zinc-Sodium Phosphate Glasses, *J. Rare Earths*, 2019, **37**(3), p 253–259. https://doi.org/10.1016/j.jre.2018.06.006
14. K.S. Shaaban, E.A.A. Wahab, E.R. Shaaban et al., Electronic Polarizability, Optical Basicity and Mechanical Properties of Aluminum Lead Phosphate Glasses, *Opt. Quant. Electron*, 2020, **52**, p 125. https://doi.org/10.1007/s11082-020-2191-3
15. A.A. El-Rehim, H. Zahran, I. Yahia et al., Radiation, Crystallization, and Physical Properties of Cadmium Borate Glasses, *Silicon*, 2020 https://doi.org/10.1007/s12633-020-00798-3
16. H.A. Saudi, W.M. Abd-Allah and K.S. Shaaban, Investigation of Gamma and Neutron Shielding Parameters for Borosilicate Glasses Doped Europium Oxide for the Immobilization of Radioactive Waste, *J*

Mater Sci: Mater Electron, 2020, **31**(9), p 6963–6976. https://doi.org/10.1007/s10854-020-03261-6
17. E.A. Abdel Wahab, A.A. El-Maaref, Kh.S. Shaaban, J. Börcsök and M. Abdelawwad, Lithium cadmium phosphate glasses doped Sm3+ as a host material for near-IR laser applications, *Opt. Mater.*, 2020 https://doi.org/10.1016/j.optmat.2020.110638
18. K.S. Shaaban, M.S.I. Koubisy, H.Y. Zahran et al., Spectroscopic Properties, Electronic Polarizability, and Optical Basicity of Titanium-Cadmium Tellurite Glasses Doped with Different Amounts of Lanthanum, *J. Inorg. Organomet. Polym.*, 2020 https://doi.org/10.1007/s10904-020-01640-4
19. A. Makehima, Y. Tamura and T. Sakaino, Elastic Moduli and Refractive Indices of Aluminosilicate Glasses Containing Y_2O_3, La_2O_3, and TiO_2, *J. Am. Ceram. Soc.*, 1978, **61**(5–6), p 247–249. https://doi.org/10.1111/j.1151-2916.1978.tb09291.x
20. K.S. Shaaban, E.S. Yousef, S.A. Mahmoud et al., Mechanical, Structural and Crystallization Properties in Titanate Doped Phosphate Glasses, *J. Inorg. Organomet. Polym*, 2020 https://doi.org/10.1007/s10904-020-01574-x
21. K.S. Shaaban and E.S. Yousef, Optical Properties of Bi_2O_3 Doped Boro Tellurite Glasses and Glass Ceramics, *Optik Int. J. Light Electron Opt.*, 2020, **203**, p 163976. https://doi.org/10.1016/j.ijleo.2019.163976
22. A.F.A. El-Rehim, K.S. Shaaban, H.Y. Zahran et al., Structural and Mechanical Properties of Lithium Bismuth Borate Glasses Containing Molybdenum (LBBM) Together with their Glass-Ceramics, *J. Inorg. Organomet. Polym.*, 2020 https://doi.org/10.1007/s10904-020-01708-1
23. R.S. Gedam and D.D. Ramteke, Synthesis and Characterization of Lithium Borate Glasses Containing La_2O_3, *Trans. Indian Inst. Met.*, 2012, **65**, p 31–35. https://doi.org/10.1007/s12666-011-0107-4
24. S. Kaewjaeng, S. Kothan, W. Chaiphaksa, N. Chanthima, R. Raja Ramakrishna, H.J. Kim and J. Kaewkhao, High Transparency La_2O_3-CaO-B_2O_3-SiO_2 Glass for Diagnosis X-Rays Shielding Material Application, *Radiat. Phys. Chem.*, 2019, **160**, p 41–47. https://doi.org/10.1016/j.radphyschem.2019.03.018
25. R. Rajaramakrishna, S. Karuthedath, R.V. Anavekar and H. Jain, Nonlinear Optical Studies of Lead Lanthanum Borate Glass Doped with Au Nanoparticles, *J. Non-Cryst. Solids*, 2012, **358**(14), p 1667–1672. https://doi.org/10.1016/j.jnoncrysol.2012.04.031
26. Y. Yamamoto, K. Kita, K. Kyuno and A. Toriumi, Structural and electrical properties of HfLaOx films for an amorphous high-k gate insulator, *Appl. Phys. Lett.*, 2006, **89**(3), p 032903. https://doi.org/10.1063/1.2227630
27. A.M. Fayad, W.M. Abd-Allah and F.A. Moustafa, Effect of Gamma Irradiation on Structural and Optical Investigations of Borosilicate Glass Doped Yttrium Oxide, *Silicon*, 2018, **10**, p 799–809. https://doi.org/10.1007/s12633-016-9533-6
28. K. Singh, N. Gupta and O.P. Pandey, Effect of Y_2O_3 on the crystallization behavior of SiO_2–MgO–B_2O_3–Al_2O_3 glasses, *J Mater Sci*, 2007, **42**, p 6426–6432. https://doi.org/10.1007/s10853-006-1188-z
29. V. Kumar, O.P. Pandey and K. Singh, Effect of A_2O_3 (A = La, Y, Cr, Al) on Thermal and Crystallization Kinetics of Borosilicate Glass Sealants for Solid Oxide Fuel Cells Glasses, *Ceram Int*, 2010, **36**(5), p 1621–1626. https://doi.org/10.1016/j.ceramint.2010.02.040
30. S. Singh, G. Kalia and K. Singh, Effect of Intermediate Oxide (Y_2O_3) on Thermal, Structural and Optical Properties of Lithium Borosilicate Glasses, *Mol. Struct.*, 2015, **1086**, p 239–245. https://doi.org/10.1016/j.molstruc.2015.01.031
31. E.A. AbdelWahab, M.S.I. Koubisy, M.I. Sayyed, K.A. Mahmoud, A.F. Zatsepin, S.A. Makhlouf and K.S. Shaaban, Novel Borosilicate Glass System: Synthesis Average Electronics Polarizability Optical Basicity and Gamma-Ray Shielding Features, *J. Non-Cryst. Solids*, 2020 https://doi.org/10.1016/j.jnoncrysol.2020.120509
32. E. Şakar and Özpolat, Öü.Fı., Alım, Bü., Sayyed, M.I., Kurudirek, M., , PhyX / PSD: Development of a User Friendly Online Software for Calculation of Parameters Relevant To Radiation Shielding and Dosimetry, *Radiat. Phys. Chem.*, 2020, **166**, p 108496. https://doi.org/10.1016/j.radphyschem.2019.108496
33. E.A. Abdel Wahab, K.S. Shaaban and E.S. Yousef, Enhancement of Optical and Mechanical Properties of Sodium Silicate Glasses Using Zirconia, *Opt. Quant. Electron*, 2020, **52**, p 458. https://doi.org/10.1007/s11082-020-02575-3
34. A.A. El-Maaref, E.A.A. Wahab, K.S. Shaaban, M. Abdelawwad, M.S.I. Koubisy, J. Börcsök and E.S. Yousef, Visible and mid-infrared spectral emissions and radiative rates calculations of Tm^{3+} doped BBLC glass, *Spectrochim. Acta Part A Mol. Biomol. Spectrosc.*, 2020 https://doi.org/10.1016/j.saa.2020.118774
35. A.F.A. El-Rehim, H.Y. Zahran, I.S. Yahia et al., Physical, Radiation Shielding and Crystallization Properties of Na_2O-Bi_2O_3- MoO_3-B_2O_3-SiO_2-Fe_2O_3 Glasses, *Silicon*, 2020 https://doi.org/10.1007/s12633-020-00827-1
36. K.S. Shaaban and Y.B. Saddeek, Effect of MoO_3 Content on Structural, Thermal, Mechanical and Optical Properties of (B_2O_3-SiO_2-Bi_2O_3-Na_2O-Fe_2O_3) Glass System, *Silicon*, 2017, **9**(5), p 785–793. https://doi.org/10.1007/s12633-017-9558-5
37. A.K. Varshneya, *Fundamentals of Inorganic Glasses*, Academic Prese Limited, Cambridge, 1994, p 33
38. K.M. Mahmoud and Y.S. Rammah, Investigation of gamma-ray shielding capability of glasses doped with Y, Gd, Nd, Pr and Dy rare earth using MCNP-5 code, *Phys. B*, 2019 https://doi.org/10.1016/j.physb.2019.411756
39. K.S. Shaaban, H.Y. Zahran, I.S. Yahia et al., Mechanical and Radiation-Shielding Properties of B_2O_3–P_2O_5–Li_2O–MoO_3 Glasses, *Appl. Phys. A*, 2020, **126**(10), p 804. https://doi.org/10.1007/s00339-020-03982-9
40. R.M. El-Sharkawy, K.S. Shaaban, R. Elsaman, E.A. Allam, A. El-Taher and M.E. Mahmoud, Investigation of Mechanical and Radiation Shielding Characteristics of Novel Glass Systems with the Composition xNiO-20ZnO-60B_2O_3-(20–x) CdO Based on Nano Metal Oxides, *J. Non-Cryst. Solids*, 2019, **528**, p 119754. https://doi.org/10.1016/j.jnoncrysol.2019.119754
41. S. Kaewjaeng, S. Kothan, W. Chaiphaksa, N. Chanthima, R. Rajaramakrishna, H.J. Kim and J. Kaewkhao, High Transparency La_2O_3-CaO-B_2O_3-SiO_2 Glass for Diagnosis X-rays Shielding Material Application, *Radiat. Phys. Chem.*, 2019 https://doi.org/10.1016/j.radphyschem.2019.03.018
42. E. Kavaz and N.Y. Yorgun, Gamma Ray Buildup Factors of Lithium Borate Glasses Doped With Minerals, *J. Alloy. Compd.*, 2018, **752**, p 61–67. https://doi.org/10.1016/j.ceramint.2019.05.028
43. P. Kaur, D. Singh and T. Singh, Heavy Metal Oxide Glasses as Gamma Rays Shielding Material, *Nucl. Eng. Des.*, 2016, **307**, p 364–376. https://doi.org/10.1016/j.nucengdes.2016.07.029
44. H.O. Tekin, E. Kavaz, A. Papachristodoulou, M. Kamislioglu, O. Agar, E.E. Altunsoy Guclu, O. Kilicoglu and M.I. Sayyed, Characterization of SiO_2–PbO–CdO–Ga_2O_3 Glasses for Comprehensive Nuclear Shielding Performance: Alpha, Proton, Gamma, Neutron Radiation, *Ceram. Int.*, 2019, **45**(15), p 19206–19222. https://doi.org/10.1016/j.ceramint.2019.06.168